Nano Research
2023, 16(4): 5873–5879

ISSN 1998-0124 CN 11-5974/O4
https://doi.org/10.1007/s12274-021-4040-5

Research Article

Engineering surface strain for site-selective island growth of Au on anisotropic Au nanostructures

Fan Yang[1], Ji Feng[1], Jinxing Chen[1,†], Zuyang Ye[1], Jihua Chen[2], Dale K. Hensley[2], and Yadong Yin[1] (✉)

[1] *Department of Chemistry, University of California, Riverside, California 92521, USA*
[2] *Center for Nanophase Materials Sciences, Oak Ridge National Laboratory, Oak Ridge, Tennessee 37831-6494, USA*
[†] *Present addtess: Institute of Functional Nano & Soft Materials, Jiangsu Key Laboratory for Carbon-Based Functional Materials & Devices, Soochow University, Suzhou 215123, China*

Received: 16 August 2021 / **Revised:** 15 November 2021 / **Accepted:** 4 December 2021

ABSTRACT

Controlled growth of islands on plasmonic metal nanoparticles represents a novel strategy in creating unique morphologies that are difficult to achieve by conventional colloidal synthesis processes, where the nanoparticle morphologies are typically determined by the preferential development of certain crystal facets. This work exploits an effective surface-engineering strategy for site-selective island growth of Au on anisotropic Au nanostructures. Selective ligand modification is first employed to direct the site-selective deposition of a thin transition layer of a secondary metal, e.g., Pd, which has a considerable lattice mismatch with Au. The selective deposition of Pd on the original seeds produces a high contrast in the surface strain that guides the subsequent site-selective growth of Au islands. This strategy proves effective in not only inducing the island growth of Au on Au nanostructures but also manipulating the location of grown islands. By taking advantage of the iodide-assisted oxidative ripening process and the surface strain profile on Au nanostructures, we further demonstrate the precise control of the islands' number, coverage, and wetting degree, allowing fine-tuning of nanoparticles' optical properties.

KEYWORDS

plasmonic, Au nanorods, island growth, seed-mediated growth, site-selective

1 Introduction

Plasmonic nanoparticles have attracted great attention due to their unique optical properties and potentials in a wide range of applications such as catalysis [1], sensing [2], and biomedicine [3]. Over the past few decades, synthetic protocols of plasmonic nanoparticles with controllable sizes and morphologies have been heavily investigated [4–7]. The relationship between the particle morphologies and their optical properties has been established. Among the reported methods, seed-mediated growth has proved to be an efficient strategy to obtain monodispersed nanocrystals with well-controlled shapes by independently manipulating the seed crystal structure and the growth kinetics [8, 9]. In recent research, the scope of seed-mediated methods has expanded from the facet-directed shape control to creating more complex nanostructures by exploring novel growth pathways [10–16]. For example, the growth of islands on seeds could produce secondary features challenging to achieve in the traditional layer-by-layer deposition [17]. The island growth can be typically observed in bimetallic systems where the depositing metal has a relatively large lattice mismatch with the substrate. It has also been reported that the island growth can be initiated on metals with a low lattice mismatch or in monometallic systems by creating a highly strained surface with strongly bound surfactants [11, 18, 19], proving efficient in producing nanostructures not accessible by direct colloidal synthesis routes. Despite these successes, achieving a high degree of control of the island features such as the number, location, and wetting degree, has remained a great challenge, especially on those with anisotropic shapes. In contrast, such precise structural tailoring is highly desirable for the fundamental study of the morphology–optical property relationship and the practical applications of the plasmonic nanostructures.

This work demonstrates that the surface strain profile on Au nanostructures can be manipulated with a combination of selective ligand modification and lattice-mismatch induced by a transition layer of another metal to achieve tunable growth of Au islands on the surface of Au nanostructures. Specifically, we employ the anisotropic modification of thiol-terminated poly(ethylene glycol) (PEGSH) to change the interfacial energy profile on Au nanorods (AuNRs), confining the deposition of a Pd transition layer on the desired sites on AuNRs. The strain difference in ligand-modified and Pd-coated regions provides a powerful templating effect to guide the further deposition of Au atoms and their overgrowth into islands. By controlling the KI concentration, growth solution amount, PEGSH to Au ratio, and polyvinylpyrrolidone (PVP) concentration during synthesis, the number, size, distance, and wetting degree of islands can be systematically tuned, achieving precise tailoring of the localized surface plasmon resonance (LSPR) properties of obtained nanostructures. Furthermore, this method can be extended to other Au nanostructures such as nanoplates, nanocubes, and rhombic dodecahedrons, showing the versatility of the site-selective island growth strategy.

Address correspondence to yadong.yin@ucr.edu

2 Results and discussion

The site-selective island growth of Au on AuNRs was performed by first modifying AuNRs with PEGSH, overcoating the modified AuNRs with a thin layer of Pd, and then using the resulting Au@Pd nanorods (Au@PdNRs) as seeds for further growth. The AuNRs were originally capped with hexadecyltrimethylammonium bromide (CTAB) during their synthesis. It has been reported that at a moderate concentration, PEGSH can selectively modify the tips of AuNRs because the packing density of CTAB on the tips of AuNRs is lower than that on the sides [20, 21]. Herein, we take advantage of the anisotropic modification of PEGSH to manipulate the deposition of Pd on the AuNRs, which further influences the growth of Au islands. Figure 1(a) illustrates the various possible nanostructures by tuning the growth modes of islands on AuNRs through anisotropic PEGSH modification and Pd deposition. The growth mode of Pd on Au nanorods is determined by the overall surface energy [22]

$$\Delta\gamma = \gamma_A + \gamma_{interfacial} + \gamma_{strain} - \gamma_B$$

where $\Delta\gamma$ is the overall excess energy; γ_A and γ_B are the surface energy of metal A and B in solution, respectively; $\gamma_{interfacial}$ is the interfacial energy between metal A and B; γ_{strain} is the energy introduced by crystal strain due to the crystal mismatch between metal A and B. A lower overall excess energy indicates a higher tendency for metal A to wet the surface of B, favoring the epitaxial growth of A on B. In contrast, higher excess energy suggests that the epitaxial growth of metal A on B is not thermodynamically favored. Therefore, controlling the deposition of Pd on AuNRs can be achieved by tuning the overall excess energy of different regions through selective ligand modification [23]. Without PEGSH modification, the tips of the AuNRs had higher surface energy due to the lower packing density of CTAB on the tips of AuNRs, which became the preferential sites of Pd deposition to produce Au@Pd_{0PEGSH}NRs. When AuNRs were modified with PEGSH, the strong bonding between Au and thiol groups increased the interfacial strain between Au and Pd. Due to the considerable lattice mismatch between Au and Pd (~ 4.6%), increasing interfacial strain, even by a small degree, is expected to change the deposition behavior of Pd [24]. At a low PEGSH/Au molar ratio of 0.01 (calculated based on thiol group to Au ratio), the strain induced by the Au–S bonds compensated for the strain difference originating from different packing densities of CTAB; therefore, Pd deposited uniformly on AuNR surface to produce Au@$Pd_{0.01PEGSH}$NRs. When PEGSH/Au ratio was further increased to 0.1, the interfacial strain between Pd and Au was greatly increased, changing the surface strain profile. The excess energy $\Delta\gamma$ on the tips was higher than that in the middle. As a result, the deposition of Pd was confined in the middle region of the AuNRs, where the PEGSH modification was limited by the densely packed CTAB, yielding Au@$Pd_{0.1PEGSH}$NRs. Although the thin Pd layer was not visible in the transmission electron microscopy (TEM) images, the different Pd distribution profiles were reflected in the ultraviolet–visible (UV–vis) spectra of the three Au@Pd nanorods. As shown in Fig. S1 in the Electronic Supplementary Material (ESM), the longitudinal peak of the Au@Pd_{0PEGSH}NRs redshifted compared to the original AuNRs, while with increasing PEGSH/Au ratio, the plasmonic peak of the Au@PdNRs blueshifted. The simulated spectra of the Au@PdNRs with tip, uniform, and side deposition (Fig. S2 in the ESM) matched our experimental results well, confirming the preferential distribution of Pd proposed in Fig. 1(a). The elemental mapping result of Au@Pd_{0PEGSH}NRs (Fig. 1(f)) also confirms that Pd covers the entire AuNRs surface but with a greater thickness at both tips, which is consistent with our simulation model.

The island growth on as-prepared Au@PdNRs was initiated by adding a growth solution containing $HAuCl_4$, L-ascorbic acid (AA), and KI in the presence of PVP as the surfactant. To study the influence of CTAB during island growth, we performed a ligand exchange process according to previously reported procedures to change the ligands on Au@PdNRs into citrates [25], which were confirmed by the Fourier-transform infrared (FTIR) spectrum and zeta-potential measurements (Fig. S3 in the ESM). The ripening process promoted by the addition of KI played an important role in the site selectivity of island growth, as it eliminated the unstable small islands through oxidative etching and promoted the growth of the remaining islands to reduce surface area and overall surface energy. When Au@Pd_{0PEGSH}NRs were used as seeds, the tips of the nanorods had a higher crystal strain due to the thicker Pd coating. As a result, the islands on the tips were highly strained and thus etched during ripening. The growth of islands mainly happened on the side of the nanorods, as shown in the TEM images (Fig. 1(b)), since the islands on the sides had a lower overall excess energy. When Au@$Pd_{0.01PEGSH}$NRs were subjected to overgrowth, due to the uniform distribution of Pd, the island growth showed no preference, and random deposition of islands on both sides and tips of the Au@$Pd_{0.01PEGSH}$

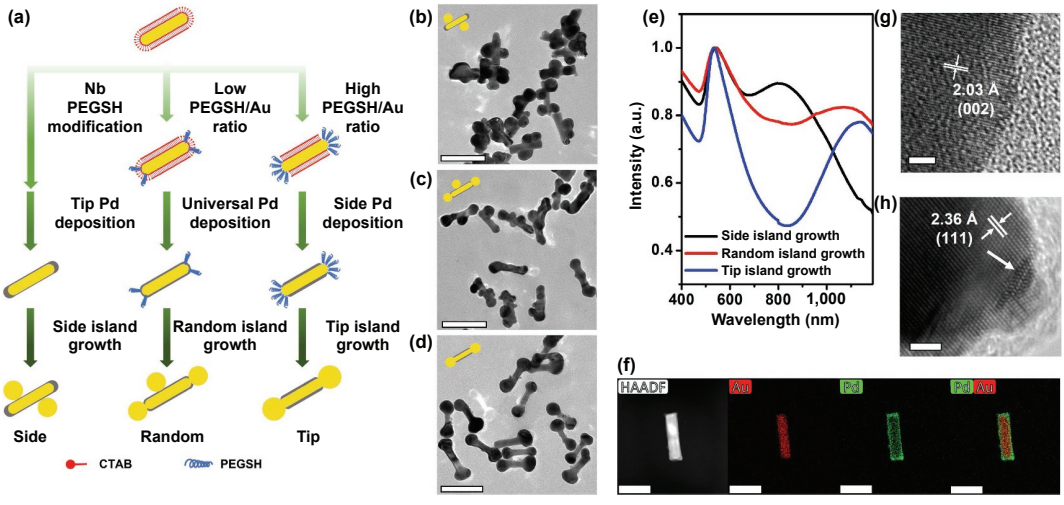

Figure 1 (a) Scheme showing the tuning of island growth locations. (b)–(d) TEM images of (b) side, (c) random, and (d) tip island growth on AuNRs. Scale bars: 50 nm. (e) UV–vis–NIR spectra of overgrown AuNRs. (f) HADDF-STEM image and EDS elemental mapping of Au@Pd_{0PEGSH}NRs. Scale bars: 50 nm. (g) and (h) HRTEM images showing small Au islands on (g) Au@PEGSHNRs and (h) Au@Pd_{0PEGSH}NRs. Scale bars: 2 nm.

NRs can be observed (Fig. 1(c)). For Au@$Pd_{0.1PEGSH}$NRs, the preferential deposition of Pd in the middle region created two areas with significant strain differences. Although the Au–S bond also increased the interfacial energy between the newly deposited islands and the original Au surface, the strain introduced by the lattice mismatch between Pd and Au was far more significant. As a result, the islands grown on the sides were etched during ripening, and the Au atoms were re-deposited onto the tips. After overgrowth, islands were deposited on the exposed tips of Au@$Pd_{0.1PEGSH}$NRs, forming dumbbell-like structures (Fig. 1(d)).

To verify whether the selective Pd deposition was due to the thiol to Au binding or the steric hindrance provided by the polymers, we performed the selective island growth on AuNRs with modification of cysteine and mercaptoacetic acid, both of which were small molecules containing thiol groups. As shown in Figs. S4(a) and S4(b) in the ESM, the dumbbell-like structures were obtained in both cases, suggesting that the selective Pd deposition could be achieved with thiol-containing chemicals, regardless of the molecule size. Therefore, the site-selective island growth could be attributed to the Au–S bond instead of the steric hindrance of the ligand. To further confirm our conclusion, we modified AuNRs with PEG terminated with an amino group ($PEGNH_2$) and then performed Pd coating and island growth. The result indicates side island growth only (Fig. S4(c) in the ESM), suggesting that the Pd distribution was not affected by $PEGNH_2$. Although $PEGNH_2$ has the same bulky polymer chain as PEGSH, the weak amino–Au interaction cannot induce enough surface strain to affect Pd deposition, producing structures similar to the case without ligand modification.

The surface strain difference induced by the thiol group and Pd deposition was further studied by depositing a small amount of Au on AuNRs completely modified with PEGSH (Au@PEGSHNRs) and Au@Pd_{0PEGSH}NRs. While Au grew into small islands on both nanorods due to the increased overall surface strain, distinct differences could be observed. As shown in the high-resolution TEM (HRTEM) of the small islands on Au@PEGSHNRs (Fig. 1(g)), despite growing into small islands, the newly deposited Au island still followed the crystal structure of the original AuNRs, indicating a relatively low surface strain on PEGSH modified surface. In Fig. 1(h), however, when Au was deposited on Au@Pd_{0PEGSH}NRs, stacking fault could be clearly observed at the connection between the Au island and the original nanorod, suggesting that the Pd coated Au surface had a high surface strain. In addition, the Au islands on Au@PEGSHNRs had small contact angles (typically ranging from 10° to 20°) with an average of 17.6° (Figs. S5(a) and S5(c) in the ESM), while the contact angles in the case of Au@Pd_{0PEGSH}NRs ranged from 70° to 100°, with an average of 84.7° (Figs. S5(b) and S5(d) in the ESM). The contact angle θ can be correlated to the surface strain with the following equation

$$\gamma_{sub} = \gamma_{interfacial} + \gamma_{island}\cos\theta$$

where γ_{sub}, $\gamma_{interfacial}$, and γ_{island} are the surface energies of the substrate, between the substrate and the islands, and the islands, respectively [26]. A higher contact angle indicated higher interfacial energy between the nanorod surface and the newly deposited Au islands. Although the contact angles obtained from TEM images cannot be directly used to quantify the surface strain of Au nanocrystal surfaces, the statistical results of the contact angles can still be meaningful for the qualitative comparison of the surface strain difference on thiol modified and Pd coated surface. It was clearly shown that the Pd coated surface had a higher surface strain than PEGSH modified ones.

As mentioned above, I^- can promote the Ostwald ripening of small Au nanoparticles in seed-mediated synthesis by forming I_3^- to oxidize Au nanoparticles according to reactions below

$$2I^- + O_2 + 4H^+ = I_2 + 2H_2O$$

$$I_2 + I^- = I_3^-$$

$$2Au + I_3^- + I^- = 2AuI_2^-$$

In this work, we varied the I^- to $HAuCl_4$ ratio in the growth solution to control the number of islands formed on a single nanorod. As shown in Figs. S6(a) and S6(b) in the ESM, we achieved the growth of multiple islands or a single island on each Au@Pd_{0PEGSH}NR by controlling the KI/$HAuCl_4$ ratio in the growth solution. With a high KI ratio, the oxidative etching of small islands with higher surface energies was greatly accelerated, and fewer islands would survive from the etching. Once Au re-deposited on one of the islands, it became a preferred deposition site for further deposition, forming a single island on each nanorod. With anisotropic PEGSH modification, the deposition of Au on the tips was preferred due to the overall excess energy on the PEGSH modified tips. With a KI/$HAuCl_4$ ratio of 10, islands would grow on both sites with an equal chance, and the typical dumbbell-like structures could be obtained (Fig. 1(d)). When the overgrowth was performed without the addition of KI, an overall overgrowth of Au@$Pd_{0.1PEGSH}$NRs could be observed (Fig. S7(a) in the ESM). It is interesting to find in the magnified images of overgrown Au@$Pd_{0.1PEGSH}$NRs without KI addition (Fig. S8 in the ESM) that the overgrown nanorods can be clearly divided into two regions. The tips modified with PEGSH grew into smooth crystals and showed clear facets. On the other hand, the overgrown crystal in the middle had rough surfaces, showing the characteristics of island growth. The different crystal growth behaviors on the tips and side of the nanorods provide another evidence of the surface strain difference between the PEGSH-modified tips and the Pd-covered side. When KI/$HAuCl_4$ was added to the growth solution with a small molar ratio of 5, the etching of small islands was relatively slow, giving a higher chance to preserve more growth sites. As a result, a third island can be observed in the middle of the nanorods, as shown in Fig. S7(b) in the ESM. When the KI/$HAuCl_4$ ratio was increased to 40, the oxidative etching was greatly promoted, growing islands on only one tip of the nanorods (Fig. S7(c) in the ESM).

The LSPR peak of the as-prepared dumbbell-like Au nanorods (AuDBs) was at 1,144 nm, falling in the second near-infrared (NIR-II) window for photothermal therapy applications. Although the potential of dumbbell-like structures in photothermal therapies has been proved [27, 28], it has been challenging to fine-tune the resonance wavelength to match the laser wavelength due to the lack of tuning parameters in the conventional kinetically controlled synthesis. Our selective PEGSH modification and Pd deposition strategy greatly amplified the surface strain difference between the tips and the sides originated from the difference in the packing density of CTAB, thus inducing a robust templating effect resembling hard templates. The main difference between the two strategies is that instead of physical blockage, which results in a fixed structure, the surface strain difference brings more flexibility since the surface strain of each region can be changed to produce more complex structures. Several morphological features of the AuDBs can be tuned to change the optical properties at different levels. For example, the size of the overgrown tips greatly affected the longitudinal resonance of the AuDBs. By adjusting the amount of growth solution added into the system, the size of the overgrown tips could be varied (Figs. 2(a)–2(d)). And as seen in the ultraviolet–visible–near-infrared (UV–vis–NIR) spectra (Fig. 2(e)), the longitudinal peaks of the AuDBs redshifted with increasing tip sizes. The longitudinal peak was very sensitive to the size of the tips and showed a nearly linear relationship with

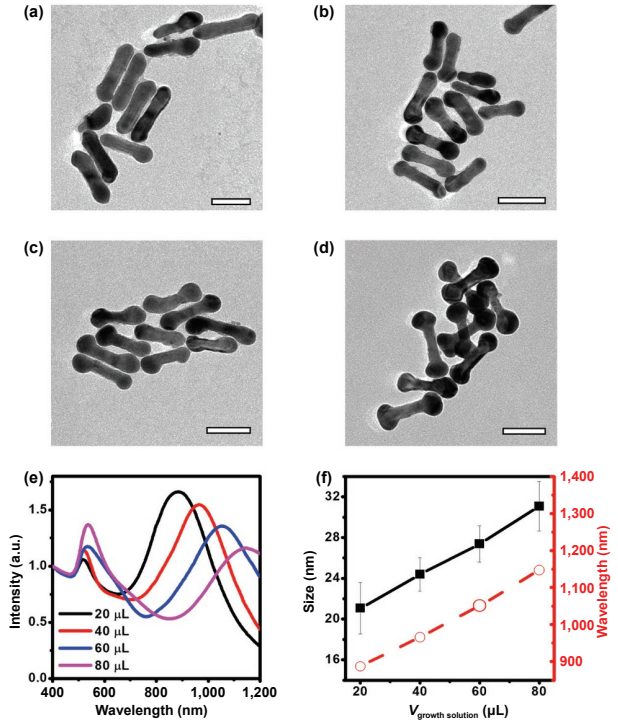

Figure 2 (a)–(d) TEM images of AuDBs synthesized by controlling the amount of the growth solution: (a) 20 μL, (b) 40 μL, (c) 60 μL and (d) 80 μL. Scale bars: 50 nm. (e) Corresponding UV–vis–NIR spectra of the AuDBs dispersion. (f) Dependence of the tip size and the resonance wavelength of the longitudinal mode on the amount of growth solution.

increasing tip sizes (Fig. 2(f)). The LSPR peak can be tuned in a wide range from 930 to 1,144 nm by simply changing the amount of growth solution. As expected, the intensity of the transverse LSPR peak of the AuDBs also dramatically increased with the increasing size of the overgrown tips.

The next level of optical tuning could be achieved by manipulating the distance between the two islands, which was made possible by controlling the coverage of Pd on AuNRs using the PEGSH/Au ratio to effectively determine the distance between the two overgrown tips. More specifically, with increasing PEGSH/Au ratio during the anisotropic modification, more area was modified with PEGSH, limiting the distribution of Pd towards the middle of the AuNRs. As a result, the distance between two overgrown tips was reduced during island growth (Figs. 3(a)–3(d)). As shown in Fig. 3(f), the distance between islands showed a steady decreasing trend proportional to the PEGSH ratio. In contrast, the overall length of the AuDBs decreased at a much slower pace. The UV–vis–NIR spectra of the as-prepared AuDBs blueshifted from 1,151 to 1,095 nm with increasing PEGSH ratio due to the decreased distance between two islands, as shown in Fig. 3(e). Simulation results (Fig. S9(a) in the ESM) also confirmed that, with the same overall length, a decrease in island distance would result in a blueshift of the longitudinal peak of AuDBs. By comparing the simulated electric field distribution around AuDBs (Figs. S9(b)–S9(e) in the ESM) with different distances between two islands, we hypothesized that blueshift resulted from decreased effective dipole distance with decreasing island distances, as a similar phenomenon has been reported by Wang et al. [29]. The island distance on overgrown nanorods offered another parameter for fine-tuning the plasmonic resonance.

The plasmonic peak of the AuDBs can be further tuned by controlling the wetting degree of the islands using surfactants. As illustrated above, the site selectivity originated from the surface strain difference between the thiol modified tips and the Pd coated

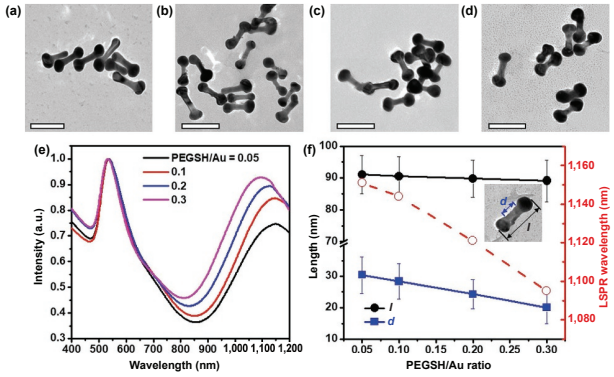

Figure 3 (a)–(d) TEM images showing controlled synthesis of AuDBs with different PEGSH/Au ratios: (a) 0.05, (b) 0.1, (c) 0.2 and (d) 0.3. Scale bars: 50 nm. (e) Corresponding UV–vis–NIR spectra of AuDBs. (f) Dependence of the distance between islands, overall length, and the LSPR wavelength of the longitudinal mode of AuDBs on the PEGSH/Au ratio.

side. PVP as a surfactant is expected to reduce the surface strain difference between the two regions, thus changing the wetting degree of the islands on the AuNRs. As shown in Figs. 4(a)–4(d), with increasing PVP concentration, the curvature at the connection of the islands and the AuNRs gradually decreased. It is worth highlighting that without PVP in the system, island growth was only observed on one tip of the nanorods (Fig. 4(a)). The addition of PVP stabilized the newly grown small islands and slowed the oxidative etching process. This effect was confirmed by observing the ripening of 2–3 nm Au seeds into large particles of ~ 35–65 nm after stirring for 1 h in the presence of KI and the absence of PVP (Fig. S10(b) in the ESM). By adding PVP with increasing concentrations, the ripening rate of the Au seeds was greatly reduced, and their final size decreased (Figs. S10(c)–S10(f) and S11 in the ESM). In contrast to the case aged without PVP, where a sharp plasmonic peak corresponds to large Au nanospheres, those aged with PVP displayed broad plasmonic peaks, proving the protecting role of PVP during the ripening process (Fig. S12 in the ESM). The addition of PVP limited the oxidative etching process, allowing the deposition of Au on both nanorod tips. As shown in the spectra of AuDBs synthesized with PVP concentration at 0.01%, 0.1%, and 2.5% (Fig. 4(e)), the gradual descending of the curvature resulted in a slight blueshift in the LSPR peak of AuDBs, which matched the results simulated based on the measured dimensions (Fig. 4(f)). By comparing the electric field distribution of AuDBs with a radius of curvature at the connection of 2 and 18 nm, we found the enhanced electric field distributed more evenly toward the center of the dumbbell structure, resulting in a decrease in the distance between effective dipoles. By combining the three key factors of AuDBs (tip size, distance, and wetting degree), the LSPR peak of the AuDBs can be tuned with high precision while maintaining a wide tuning range (Fig. S13 in the ESM), making it possible to match the plasmonic property with the excitation wavelength for various applications.

The key to the site-selective island growth strategy is amplifying the difference in surface strain by the difference in the packing density of CTAB on tips and sides of AuNRs. This principle can be applied to other halide-capped Au nanostructures with different local surface curvatures, for example, on the faces and the corners of Au nanoplates (Figs. S14(c) and S14(d) in the ESM) and nanocubes (Figs. S14(c) and S14(d) in the ESM). Without PEGSH modification, the growth of islands was limited on the faces of the Au nanocubes, while island growth on the tips was achieved with PEGSH modification at a PEGSH/Au ratio of 0.1. The selective PEGSH modification was also extended to Au nanostructures such as nanoplates (Fig. 5(b)), nanocubes

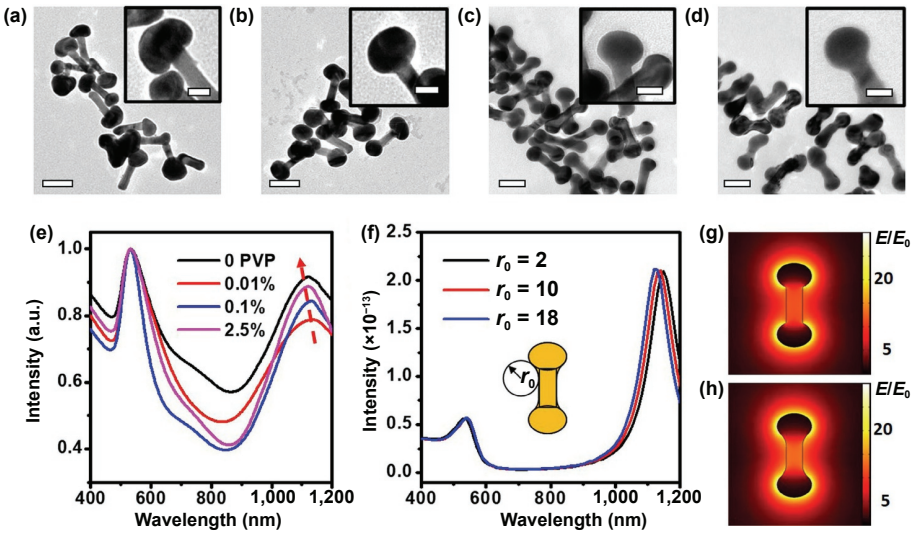

Figure 4 (a)–(d) TEM images showing the controlled synthesis of AuDBs using (a) 0%, (b) 0.01%, (c) 0.1% and (d) 2.5% PVP. Scale bars: 50 nm. Insets are magnified images at the connection of the island and nanorods. Scale bars in insets are 20 nm. (e) Corresponding UV–vis–NIR spectra of AuDBs synthesized with different PVP concentrations. (f) Simulated spectra of AuDBs with curvature radius at the connection of 2, 10, and 18 nm. (g) and (h) electric field distribution of AuDBs with a curvature radius of 2 nm (g) and 18 nm (h) at their resonance wavelengths.

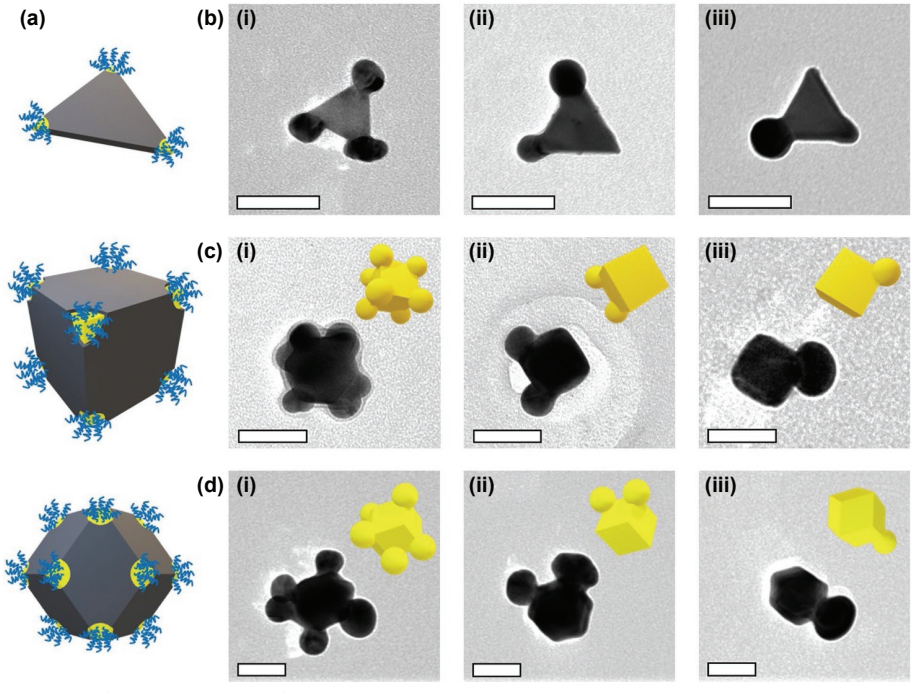

Figure 5 (a) Schematic illustration of the seeded growth of Au on the Au@$Pd_{0.1PEGSH}$PLTs, Au@$Pd_{0.1PEGSH}$CBs, and Au@$PD_{0.1PEGSH}$RDs. (b) TEM images showing island growth on Au@$Pd_{0.1PEGSH}$PLTs with (i) three, (ii) two, and (iii) one tip(s) grown. (c) TEM images showing island growth on Au@$Pd_{0.1PEGSH}$CBs with (i) seven, (ii) two, and (iii) one tip(s). Insets are the 3D models of the corresponding particles to help with the visualization of the structures. (d) TEM images showing island growth on (d) Au@$PD_{0.1PEGSH}$RDs with (i) five, (ii) two, and (iii) one tip(s). Insets are the 3D models of corresponding particles. Scale bars: 50 nm.

(Fig. 5(c)), and rhombic dodecahedrons (Fig. 5(d)). The number of islands could also be controlled by manipulating the ripening process of the small islands. Although a precise control of the number of overgrown tips remained challenging, all three Au nanostructures clearly showed a reduced number of islands with increasing KI/$HAuCl_4$ ratio in the growth solution (Fig. S15 in the ESM), proving the versatility and robustness of our proposed synthetic strategy.

3 Conclusions

In this work, we demonstrated a surface-engineering strategy to induce site-selective growth of Au islands on Au nanostructures. The growth location of the islands was controlled by creating regions with significant surface strain differences within a single nanocrystal with the combination of selective ligand modification and lattice-mismatch induced by a thin Pd transition layer. Thanks to the flexibility of this templating strategy, we achieved the independent control of the islands' structural features, including number, size, coverage, and wetting degree through four critical parameters: iodide-assisted oxidative ripening, growth solution amount, PEGSH to Au ratio, and surface strain difference which can be manipulated by PVP concentration. Our strategy led to establishing a comprehensive protocol for fine-tuning the island growth products, allowing the tailoring of novel Au nanostructures for specific requirements. Further, we demonstrated that the site-selective island growth was versatile and can be extended to other Au nanostructures (nanoplates, nanocubes, and rhombic dodecahedrons), with the island number controllable by the ripening process. Since the principle of surface

strain engineering is general, it may be extended to other nanocrystal growth systems to create new morphologies and physical properties.

4 Experimental

4.1 Synthesis of AuNRs

The Au nanorods were synthesized with a method published by Jianfang Wang with slight modification [30]. A seed solution was first prepared by adding 60 μL of freshly prepared 0.1 M $NaBH_4$ solution into 10 mL of a solution containing 0.1 M CTAB and 0.25 mM $HAuCl_4$. The mixture was stirred vigorously for 30 s, and then aged at 25 °C without disturbance for at least 30 min to remove unreacted $NaBH_4$. The growth solution was prepared by combining 40 mL 0.1 M CTAB, 2 mL 0.01 M $HAuCl_4$, 0.4 mL 0.01 M $AgNO_3$, 0.8 mL 1 M HCl and 0.32 mL 0.1 M AA in sequence. The growth of AuNRs was initiated by adding 96 μL seed solution into the growth solution. The mixture was vigorously stirred for 30 s and kept undisturbed at 25 °C for 12 h. The synthesized AuNRs were separated by centrifugation at 9,000 rpm for 30 min. The AuNRs were washed with water twice and redispersed in 20 mL 0.01 M CTAB solution to make the AuNRs concentration equal to 1 mM.

4.2 Synthesis of Au nanoplates (AuPLTs)

The hexadecyltrimethylammonium chloride (CTAC)-capped Au nanoplates were synthesized with a previously reported method by Qiao Zhang [31]. In a 50 mL flask, 20 mL of water and 4 mL of 0.1 M CTAC solution were added, followed by 375 μL of 0.01 M KI. A mixture of 400 μL 25 mM $HAuCl_4$ and 100 μL of 0.1 M NaOH was added sequentially to make a yellowish color. After injecting 400 μL of 0.064 M AA under moderate stirring, the solution turned colorless. The Au nanoplate growth was initiated with the injection of 50 μL 0.1 M NaOH. The solution was vigorously stirred for 10 s and left undisturbed for 10 min. The nanoplates were separated with centrifugation at 9,000 rpm for 10 min and redispersed in 10 mL of 0.01 M CTAB solution.

4.3 Synthesis of Au nanocubes (AuCBs) and rhombic dodecahedrons (AuRDs)

The Au nanocubes and rhombic dodecahedrons were synthesized with a method reported by Michael Huang [32]. In a 20 mL flask, 10 mL 0.1 M CTAC was added, followed by adding 250 μL 10 mM $HAuCl_4$ solution. Into the mixture, 0.45 mL of freshly prepared 0.2 M $NaBH_4$ solution was quickly injected under vigorous stirring. The seed solution was aged for 1 h at 30 °C before use.

For the growth of Au nanocubes, two vials were labeled A and B. A growth solution was prepared in each of the two vials. In each vial, 10 mL of 0.1 M CTAC was added, followed by 250 μL of 0.01 M $HAuCl_4$, and 10 μL of 0.01 M KBr were added. Finally, 90 μL of 0.04 M AA was added. To initiate the crystal growth, 45 μL seed solution was added to vial A under vigorous stirring. After 10 s, solution A turned pink, and 45 μL of solution A was injected into vial B. The mixture was stirred for 10 s and left undisturbed for 15 min. The Au nanocubes were separated by centrifugation at 7,000 rpm for 15 min and redispersed in 2.5 mL 0.01 M CTAB solution. For synthesizing Au rhombic dodecahedrons, 150 μL of 0.04 M AA instead of 90 μL was added to each growth solution.

4.4 Synthesis of Au@PdNRs

The AuNRs were first modified with PEGSH (M_w ~ 2,000) before Pd deposition. Into 5 mL of AuNRs solution, 0.5 mL of 1 mM PEGSH solution was added. The solution was stirred for 2 h for the selective modification of PEGSH on Au nanorods. The modified AuNRs were centrifuged and redispersed in 5 mL of 2 mM CTAB solution. Various amount of PEGSH solution was added to obtain AuNRs modified with different PEGSH/Au molar ratios. To initiate the Pd deposition, 500 μL 0.1 M AA and 50 μL 0.02 M H_2PdCl_4 solution were added under stirring. The mixture was stirred for 30 min before centrifugation. The Au@PdNRs were centrifuged at 9,000 rpm for 10 min to remove unreacted chemicals and redispersed in 1 mL of water.

The selective Pd deposition on other Au nanostructures (AuPLTs, AuCBs, AuRDs) was carried out with the same procedure, with slight modifications of PEGSH/Au and Pd/Au ratios. The amount of AA was adjusted proportionally according to the amount of H_2PdCl_4 added. More specifically, for AuPLTs, PEGSH/Au = 0.05 and Pd/Au = 0.1 was used, while for AuNBs and AuRD, PEGSH/Au = 0.05 and Pd/Au = 0.2 was used.

4.5 Ligand exchange of Au@PdNRs

Before island growth, the ligand of Au@PdNRs was changed from CTAB into citrate with a previously reported ligand exchange process. Generally, 1 mL of Au@PdNRs solution was added into 3 mL of ethanol. Into the mixture, 100 μL of 5% PVP (M_w ~ 10,000) solution was added and stirred for 4 h. The Au@PdNRs were then centrifuged and redispersed in 1 mL of water. Into the Au@PdNRs solution, 50 μL of diethylamine (DEA) was added and stirred for 2 h to exchange the ligand into DEA. To finally exchange the ligand into citrate, the Au@PdNRs were centrifuged and redispersed in 1 mL of water, to which 20 μL of 10 mg/mL trisodium citrate (TSC) and 40 μL of 10 mg/mL tannic acid were added. The solution was stirred for 1 h and then centrifuged to remove supernatant. The collected Au@PdNRs were redispersed in 5 mL of water.

The same ligand exchange processes were performed on other Au@Pd nanostructures (Au@PdPLTs, Au@PdCBs, and Au@PdRDs).

4.6 Island growth on Au@PdNRs

Into 0.5 mL of water, 20 μL 5 wt.% PVP solution, 50 μL 0.01 M $HAuCl_4$, 25 μL 0.2 M KI and 5 μL 0.1 M AA were added to prepare the growth solution. The above growth solution was injected into 0.5 mL of Au@PdNRs dispersion, and the mixture was stirred for 30 min. The overgrown Au@PdNRs were separated by centrifuging at 8,000 rpm for 5 min and redispersed in water for characterization. The same processes were carried out for the site-selective island growth on other An@Pd nanostructures.

4.7 Characterization

TEM images were acquired on a Philips Tecnai 12 transmission electron microscope, operating at 120 kV and a JEOL 2100 scanning TEM (STEM) operating at 200 kV. The morphology of the overgrown Au rhombic dodecahedrons was characterized by an FEI Nova NanoSEM 450 scanning electron microscope (SEM). STEM images and energy-dispersive X-ray spectroscopy (EDS) mapping profiles were collected on an FEI Talos F200X transmission electron microscope operating at 200 kV. UV–Vis spectra were measured with an Ocean Optics HR2000 CG-UV-NIR spectrometer. The UV–vis–NIR spectra were measured with a Gary 5000 double beam UV–vis–NIR spectrometer. FTIR spectra were measured with a Thermo Nicolet 6700 FTIR spectrometer.

Acknowledgements

This work was financially supported by the US National Science Foundation (CHE-1808788).

Electronic Supplementary Material: Supplementary material (simulated UV–vis spectra of Au@PdNRs, ligand exchange of Au@PdNRs, TEM images of overgrown Au@PdNRs with varied synthetic conditions, simulated spectra and electric field distribution of AuDBs, KI assisted ripening of small Au seeds, TEM images of controlled island growth on AuCBs, and statistic results of numbers of islands grown on Au nanocrystals) is available in the online version of this article at https://doi.org/10.1007/s12274-021-4040-5.

References

[1] Zhang, Z. L.; Zhang, C. Y.; Zheng, H. R.; Xu, H. X. Plasmon-driven catalysis on molecules and nanomaterials. *Acc. Chem. Res.* **2019**, *52*, 2506–2515.

[2] Li, M.; Cushing, S. K.; Wu, N. Q. Plasmon-enhanced optical sensors: A review. *Analyst* **2015**, *140*, 386–406.

[3] Khlebtsov, N. G.; Dykman, L. A. Optical properties and biomedical applications of plasmonic nanoparticles. *J. Quant. Spectrosc. Radiat. Transf.* **2010**, *111*, 1–35.

[4] Tao, A. R.; Habas, S.; Yang, P. D. Shape control of colloidal metal nanocrystals. *Small* **2008**, *4*, 310–325.

[5] Xia, Y. N.; Gilroy, K. D.; Peng, H. C.; Xia, X. H. Seed-mediated growth of colloidal metal nanocrystals. *Angew. Chem., Int. Ed.* **2017**, *56*, 60–95.

[6] Huang, X. H.; Neretina, S.; El-Sayed, M. A. Gold nanorods: From synthesis and properties to biological and biomedical applications. *Adv. Mater.* **2009**, *21*, 4880–4910.

[7] Polte, J. Fundamental growth principles of colloidal metal nanoparticles – a new perspective. *CrystEngComm* **2015**, *17*, 6809–6830.

[8] Chow, T. H.; Li, N. N.; Bai, X. P.; Zhuo, X. L.; Shao, L.; Wang, J. F. Gold nanobipyramids: An emerging and versatile type of plasmonic nanoparticles. *Acc. Chem. Res.* **2019**, *52*, 2136–2146.

[9] Chen, J. X.; Bai, Y. C.; Feng, J.; Yang, F.; Xu, P. P.; Wang, Z. C.; Zhang, Q.; Yin, Y. D. Anisotropic seeded growth of Ag nanoplates confined in shape-deformable spaces. *Angew. Chem., Int. Ed.* **2021**, *60*, 4117–4124.

[10] Jia, J.; Liu, G. Y.; Xu, W. J.; Tian, X. L.; Li, S. B.; Han, F.; Feng, Y. H.; Dong, X. C.; Chen, H. Y. Fine-tuning the homometallic interface of Au-on-Au nanorods and their photothermal therapy in the NIR-II window. *Angew. Chem., Int. Ed.* **2020**, *59*, 14443–14448.

[11] Huang, J. F.; Zhu, Y. H.; Liu, C. X.; Shi, Z.; Fratalocchi, A.; Han, Y. Unravelling thiol's role in directing asymmetric growth of Au nanorod-Au nanoparticle dimers. *Nano Lett.* **2016**, *16*, 617–623.

[12] Lee, H. E.; Kim, R. M.; Ahn, H. Y.; Lee, Y. Y.; Byun, G. H.; Im, S. W.; Mun, J.; Rho, J.; Nam, K. T. Cysteine-encoded chirality evolution in plasmonic rhombic dodecahedral gold nanoparticles. *Nat. Commun.* **2020**, *11*, 263.

[13] Ma, Y. J.; Cao, Z. Z.; Hao, J. J.; Zhou, J. H.; Yang, Z. J.; Yang, Y. Z.; Wei, J. J. Controlled synthesis of Au chiral propellers from seeded growth of Au nanoplates for chiral differentiation of biomolecules. *J. Phys. Chem. C* **2020**, *124*, 24306–24314.

[14] Tan, R. L. S.; Chong, W. H.; Feng, Y. H.; Song, X. H.; Tham, C. L.; Wei, J.; Lin, M.; Chen, H. Y. Nanoscrews: Asymmetrical etching of silver nanowires. *J. Am. Chem. Soc.* **2016**, *138*, 10770–10773.

[15] Wang, Z. X.; He, B. W.; Xu, G. F.; Wang, G. J.; Wang, J. Y.; Feng, Y. H.; Su, D. M.; Chen, B.; Li, H.; Wu, Z. H. et al. Transformable masks for colloidal nanosynthesis. *Nat. Commun.* **2018**, *9*, 563.

[16] Yip, H. K.; Zhu, X. Z.; Zhuo, X. L.; Jiang, R. B.; Yang, Z.; Wang, J. F. Gold nanobipyramid-enhanced hydrogen sensing with plasmon red shifts reaching ≈140 nm at 2 vol% hydrogen concentration. *Adv. Opt. Mater.* **2017**, *5*, 1700740.

[17] Feng, J.; Xu, D. D.; Yang, F.; Chen, J. X.; Wu, C. L. M.; Yin, Y. D. Surface engineering and controlled ripening for seed-mediated growth of au islands on Au nanocrystals. *Angew. Chem., Int. Ed.* **2021**, *60*, 16958–16964.

[18] Feng, Y. H.; He, J. T.; Wang, H.; Tay, Y. Y.; Sun, H.; Zhu, L. F.; Chen, H. Y. An unconventional role of ligand in continuously tuning of metal–metal interfacial strain. *J. Am. Chem. Soc.* **2012**, *134*, 2004–2007.

[19] Feng, Y. H.; Wang, Y. W.; He, J. T.; Song, X. H.; Tay, Y. Y.; Hng, H. H.; Ling, X. Y.; Chen, H. Y. Achieving site-specificity in multistep colloidal synthesis. *J. Am. Chem. Soc.* **2015**, *137*, 7624–7627.

[20] Wang, F.; Cheng, S.; Bao, Z. H.; Wang, J. F. Anisotropic overgrowth of metal heterostructures induced by a site-selective silica coating. *Angew. Chem., Int. Ed.* **2013**, *52*, 10344–10348.

[21] Li, F.; Wang, K.; Tan, Z. P.; Guo, C.; Liu, Y. Y.; Tan, H. Y.; Zhang, L. B.; Zhu, J. T. Solvent quality-mediated regioselective modification of gold nanorods with thiol-terminated polymers. *Langmuir* **2020**, *36*, 15162–15168.

[22] Peng, Z. M.; Yang, H. Designer platinum nanoparticles: Control of shape, composition in alloy, nanostructure and electrocatalytic property. *Nano Today* **2009**, *4*, 143–164.

[23] DeSantis, C. J.; Weiner, R. G.; Radmilovic, A.; Bower, M. M.; Skrabalak, S. E. Seeding bimetallic nanostructures as a new class of plasmonic colloids. *J. Phys. Chem. Lett.* **2013**, *4*, 3072–3082.

[24] Ding, Y.; Fan, F. R.; Tian, Z. Q.; Wang, Z. L. Atomic structure of Au-Pd bimetallic alloyed nanoparticles. *J. Am. Chem. Soc.* **2010**, *132*, 12480–12486.

[25] Fan, Q. K.; Yang, H.; Ge, J.; Zhang, S. M.; Liu, Z. J.; Lei, B.; Cheng, T.; Li, Y. Y.; Yin, Y. D.; Gao, C. B. Customizable ligand exchange for tailored surface property of noble metal nanocrystals. *Research* **2020**, *2020*, 2131806.

[26] Lewis, D. J.; Zornberg, L. Z.; Carter, D. J. D.; Macfarlane, R. J. Single-crystal Winterbottom constructions of nanoparticle superlattices. *Nat. Mater.* **2020**, *19*, 719–724.

[27] Yin, J. C.; Wu, H. N.; Wang, X.; Tian, L.; Yang, R. L.; Liu, L. Z.; Shao, Y. Z. Plasmonic nano-dumbbells for enhanced photothermal and photodynamic synergistic damage of cancer cells. *Appl. Phys. Lett.* **2020**, *116*, 163702.

[28] Zhang, Y. F.; Song, T. J.; Feng, T.; Wan, Y. L.; Blum, N. T.; Liu, C. B.; Zheng, C. Q.; Zhao, Z. Y.; Jiang, T.; Wang, J. W. et al. Plasmonic modulation of gold nanotheranostics for targeted NIR-II photothermal-augmented immunotherapy. *Nano Today* **2020**, *35*, 100987.

[29] Zhu, X. Z.; Yip, H. K.; Zhuo, X. L.; Jiang, R. B.; Chen, J. L.; Zhu, X. M.; Yang, Z.; Wang, J. F. Realization of red plasmon shifts up to ~ 900 nm by AgPd-tipping elongated Au nanocrystals. *J. Am. Chem. Soc.* **2017**, *139*, 13837–13846.

[30] Ni, W. H.; Kou, X. S.; Yang, Z.; Wang, J. F. Tailoring longitudinal surface plasmon wavelengths, scattering and absorption cross sections of gold nanorods. *ACS Nano* **2008**, *2*, 677–686.

[31] Chen, L.; Ji, F.; Xu, Y.; He, L.; Mi, Y. F.; Bao, F.; Sun, B. Q.; Zhang, X. H.; Zhang, Q. High-yield seedless synthesis of triangular gold nanoplates through oxidative etching. *Nano Lett.* **2014**, *14*, 7201–7206.

[32] Kuo, B. H.; Hsia, C. F.; Chen, T. N.; Huang, M. H. Systematic shape evolution of gold nanocrystals achieved through adjustment in the amount of $HAuCl_4$ solution used. *J. Phys. Chem. C* **2018**, *122*, 25118–25126.